Journal of Fluorescence (2019) 29:549–567
https://doi.org/10.1007/s10895-019-02367-3

ORIGINAL ARTICLE

# Enhanced Luminescence Based Response towards pH in Highly Acidic Environments by the Silver Nanoparticles and Ionic Liquids

Hacer Esra Kabak[1] · Kadriye Ertekin[2] · Merve Zeyrek Ongun[3] · Serpil Denizalti[4]

Received: 21 January 2019 / Accepted: 10 March 2019 / Published online: 27 March 2019


## Abstract

Correct measurement of the pH in highly acidic environments is still a challenge. In such conditions most of the pH indicators suffer from instability in air or leaching from host matrices due to the solubility considerations. In this work, two different fluorescent probes were used along with silver nanoparticles (AgNPs) and ionic liquid (IL) in the polymeric matrices for sensing of the pH in harsh conditions. The pH sensitivities of the probes were tested after exposure to strong acid vapors by steady-state, lifetime based and kinetic mode measurements. The sensing materials were fabricated in form of thin films and electrospun nanofibers. The ionic liquid; 1-butyl-3-methylimidazolium tetrafluoroborate was exploited as additive to enhance the stability as well as response towards pH. Spectral changes were tested in a large scale; between pH 3.00–12.00. Utilization of the dyes in ethyl cellulose and polymethyl methacrylate along with AgNPs in form of electrospun fibers resulted in many advantages such as enhanced long term stability, sensitivity and improvement in all sensor dynamics. Sensing characteristics of the offered designs were tested after exposed to vapors of HCl, $H_2SO_4$ and $HNO_3$, respectively.

**Keywords** Optical pH sensor · Strong acids · Fluorescence · AgNPs · Silver nanoparticles · Electrospinning

## Introduction

pH is probably one of the most intensively controlled parameters in industrial field, environmental studies, medical and biotechnological research. pH measurements can be used directly in the control of water quality, intra-cell research, in the monitoring of the air quality of workplaces, or it is sometimes the underlying technology in the measurement of many parameters like dissolved carbon dioxide, blood gases or glucose. On the other hand, fumes of the acids are very corrosive and their inhalation may lead to tissue destruction, gastritis, chronic bronchitis and lung damage even at low concentrations. For this reason, accurate, reliable and reproducible measurement of the pH is extremely important. However, correct measurement of the pH in highly acidic environments is still a challenge. Nowadays, fluorescence-based optical chemical sensors utilizing proton sensitive molecules have been emerged as a good alternative to the electrochemical approach. Some of them are still a part of ongoing research and some have been commercialized. However, the photo-stability and long-term stability of the pH probes is controversial and their ability to measure the pH is limited by the acidity constant or solubility considerations. Therefore, new effort is necessary to overcome these problems.

Conceptual basis of optical pH sensor design relies on absorption, or, more frequently emission based measurements [1–9]. Solutions of the well-known commercially available pH indicators of Bromophenol Blue, Methyl Orange, Bromothymol Blue, Phenolphthalein, Curcumin, Alzarin Yellow, Alizarin Red, Fluorescein and carboxyfluoresceins, HPTS (pyranine) dyes, SNARF indicators and many others have been used to detect the pH [10]. In most of the former

**Electronic supplementary material** The online version of this article (https://doi.org/10.1007/s10895-019-02367-3) contains supplementary material, which is available to authorized users.

✉ Kadriye Ertekin
kadriye.ertekin@deu.edu.tr

✉ Merve Zeyrek Ongun
merve.zeyrek@deu.edu.tr

[1] The Graduate School of Natural and Applied Sciences, Department of Chemistry, University of Dokuz Eylul, 35160, Buca, Izmir, Turkey

[2] Faculty of Sciences, Department of Chemistry, University of Dokuz Eylul, 35160, Buca, Izmir, Turkey

[3] Chemistry Technology Program, Izmir Vocational School, Dokuz Eylül University, 35160 Buca, Izmir, Turkey

[4] Faculty of Science, Department of Chemistry, University of Ege, 35100 Bornova, Izmir, Turkey

studies and in some of the recent ones the pH sensitivity of the indicator dyes has been tested and evaluated in the solution phase. Obviously the solution phase studies provided valuable information for the scientists in understanding of the protonation-deprotonation equilibria and other pH sensing dynamics. In the last three decades, combination of the indicator chemistry with the polymeric or glassy materials has been a promising development for the solid state optical chemical sensors [11–16]. As a consequence, a number of emission based experimental studies have been performed in the different forms of the solid state including thin films, fibers and nano-sclae materials. Except that of instrumentation, the indicator chemistry of such optical chemical sensors are mainly composed of a polymeric matrix material, a pH sensitive ionophore, more specifically a fluoroionophore, or a combined form of the ion carrier and dye; that acts as a fluorescent probe. Aside from instrumentation, probably, the most challenging aspect of an optical sensor design is the planning of the indicator chemistry which covers proper choice of pH sensitive indicator and compatible matrix material where the reagent dye can be adsorbed, covalently or electrostatically immobilized, or simply encapsulated that is also permeable to the analyte. Fluorescein and derivatives [1, 9, 14] porphyrin molecules, Hydroxy-3,6,8-pyrenetrisulfonate (HPTS), ion pair form of HPTS [3–8], Prussian blue *and N*-substituted polypyrroles, a combination of Ruthenium(II)-4,7-diphenyl-1,10-phenanthroline($Ru(dpp)_2$) and fluorescein [13], perylene bisimide (PBI) [15] and rhodamine dyes [16], coumarin derivatives [17], benzimidazo[2,1-a]benz[de] isoquinoline-7-one-12-carboxylic acid based fluorescent probes [18] and carbazole dyes [19] have been used as indicators in the design of the solid-state pH sensors.

In order to perform an efficient immobilization and long term stability of the indicator in the support matrix, the pH sensitive dye must be soluble and stable in the chosen material. Commonly used polymeric matrix materials in the sensor design include, polymethyl methacrylate [1], polydimethyl siloxanes, and polytetrafluoro ethylenes, polymers for molecular imprinting, organic conductive polymers, hydrogel-plasticizer emulsions [2, 4, 6, 9] substituted polypyrroles [11, 12], polyvinyl chloride and cellulose derivatives such as ethyl cellulose [19]. The sol-gel process and different types of glassy materials also provide relatively suitable support matrix for the immobilization of pH-sensitive reagents. Recently, with advances in materials fabrication and better understanding of the dynamics of the nano-scale materials, these are being used in optical sensor design as matrix materials or encapsulation moiety for the indicator dye. Understanding of the availability of nano-scale materials is a comparatively novel development in this area and future applications of the nano materials look like promising. A short summary of the recent pH sensors indicating the sensitive dye, matrix material and some other sensor characteristics including sensitivity information, working range, detection limit, response time and stability is given in Table 1.

In this work, two different fluorescent pH indicators have been encapsulated in polymeric matrices along with ionic liquid and metallic nano-particles. pH induced sensitivities and stabilities of the ($N^1E,N^2E$)-$N^1,N^2$-bis((E)-3-(4-(dimethylamino) phenyl)allylidene) ethane-1,2-diamine (SDA), and (E)-$N^1$-((E)-3-(4-(dimethylamino) phenyl)allylidene)-$N^4,N^4$-dimethylbenzene-1,4-diamine (SDC) have been investigated in ethyl cellulose (EC) and poly (methyl methacrylate) (PMMA) matrices, respectively. The polymers were chosen due to excellent proton permabilities, resistant characteristics to water and harsh conditions, protecting abilities of the indicator dyes from alterations providing an appropriate micro environment for them, and, tailoring abilities on electrospinning conditions. On the other hand, it is known that presence of the conducting metallic species like silver is effective on emissive spectral properties of nearby fluorophores. The excited fluorophores may transfer their energy to the surface plasmons of the close proximity metal particles, which subsequently re-radiate and in some cases enhance the detection ability of the molecular probe. In this work, we utilized the silver nanoparticles (AgNPs) along with ionic liquid as additives for the fabrication of polymeric pH sensitive mesoporous structures and electrospun micro or nanofibers. The pH induced sensitivities of the utilized pH dyes; (SDA and SDC) have been investigated by our working group in PVC and EC matrices, in thin film form earlier [20].

In this work, the two fluorescent probes have been proposed for the pH measurements challenging the interference effects of vapors of strong acids and other potential interferents. The sensing ability of the indicators has been tailored considering the environments occupied by acid vapors. To the best of our knowledge this is the first study utilizing the fluorescent pH probes of SDA and SDC along with the additives of AgNPs and ionic liquid in the form of electrospun nano or meso-scale polymeric fibers. Presence of the nano-scale metallic silver and ionic liquid within the matrix provided a better resolution in response and an extra immunity towards the potential interferents extending the shelf-life of the sensor materials up to 18 months.

## Experimental

### Reagents

Poly (methyl methacrylate) (PMMA) and bis-(2-ethylhexyl)phthalate (DOP), were purchased from Merck and Fluka, respectively. Ethyl cellulose (with an ethoxy content of 46%) and potassium tetrakis-(4-chlorophenyl)borate (PTCPB) were from Aldrich. Absolute ethanol (EtOH), tetrahydrofuran (THF), dichloromethane (DCM), and toluene (To) were of analytical grade and used without further purification. $NaBH_4$ and

**Table 1** A short summary of the pH sensing studies (NR: not reported, Ref.: Reference)

| Sensitive dye/ measured parameter | Matrix materials | Sensitivity/ pKa | Dynamic working range/ working range | Detection limit/ response time | Stability | Ref. |
|---|---|---|---|---|---|---|
| Polymerization of a monomeric fluorescein based green emitter with a monomeric 2 dicyanomethylene-3--cyano-4,5,5-trimethyl-2,5-dihydrofuran derived red emitter | Poly(2-hydroxyethyl methacrylate)-co-polyacryl amide with cross linker | Sensitivity (IpH 3/IpH 9), pKa for different compositions 7.73–4.60 | pH 4.0- to pH 8.0 for different compositions | NA | Good short term photostability. reversible after 6 cycles between pH 3–9 | [1] |
| Covalently attached porphyrin molecules free-base porphyrin self-assembled monolayers | 125 μm tapered fibre /Surface activation by aminopropyltrimethoxysilane | pH dependence is convincingly fitted with two linear approximations having a turning point at a pH of around 1.5. | Operates in the pH range of 0.6–3.8. | NA | NA | [2] |
| Covalently immobilized I-Hydroxy-3,6,8-pyrenetrisulfonate (HPTS) | Cellulose attached to a plastic strip | Near neutral region and in the low pH region from about pH 3 to below pH 1 | Over a broad range of pH, 0–9. | NA | NA | [3] |
| Modified 8-hydroxy-1,3,6-pyrene trisulfonic acid (HPTS) | -glycidoxy propyltrimethoxy-silane (GPTMS) and ethyltriethoxysilane (ETEOS) based sol-gel | pKa 6.28 ± 0.02 | pH 5.0 to 8.0 | Response time of 12 s. | Over the period of 3 years the pKa value remains unchanged (RSD 1.2%). | [4] |
| Ag core and pH sensitive dye (HPTS) | Ag@$SiO_2$ Core−Shell Nanoparticles | At the shell thickness of 8 nm, maximum fluorescence enhancements of 4 and 9 times were achieved | In the pH range of 5–9. | NA | When >pH 9.5, high stability in the pH range of 5–9. | [5] |
| Ion-pair of 8-hydroxypyrene 1,3,6-trisulfonic acid trisodium salt and hexadecyltrimethyl-ammonium bromide | Xerogel matrices composed of ethyltriethoxysilane and (3-glycid oxypropyl)-trimethoxy silane | Sensitivity of the probe in the pH range of 5.75 7.25: 0.56 pH − 1. pH-resolution ~ 0.07 pH unit | pH from 5.75 to 7.25 | NA | NA | [6] |
| PAA hydrogel nanoparticles loaded with HPTS dye/ two-photon intracellular pH sensing | 68 nm of PAA hydrogel nanoparticles, contain about 0.5% dye by weight | two photon calibration curve R sq. value: 0.98 single photon calibration curve: R sq. value 0.96 | Linear response in the pH range of 6 to 8. | NA | 8% and 9% dye leaching in 24 and 60 h, respectively. | [7] |
| 8-hydroxy-1,3,6-pyrene trisulfonic acid (HPTS) and 6-methacryloyl-8--hydroxy-1,3-pyrene disulfonic acid (MA-HPDS | Copolymerization of the MA-HPDS with poly(ethylene glycol) diacrylate. | p*K*a1, app = 7.003 ± 0.02 and p*K*a2, app = 9.05 ± 0.02 | pH range of 6–9, with excellent reproducibility | Rapid response to pH | Robust, sterizible with steam, well suited to bioprocess applications | [8] |
| Covalent immobilization of aminofluorescein (AF) via isocyanate or epoxy groups | Tetramethoxysilane (TMOS) and phenyltrimethoxysilane (Ph-TriMOS) | pKa: 6.62 ± 0.08. | pH range of 4–9. | The response and regeneration times 90 and 120 s, respectively. | In distilled water, buffer of pH 4.7, buffer of pH 8.3, buffer of pH 7; 0.05 and in air stable for 6 months. | [9] |

**Table 1** (continued)

| Sensitive dye/ measured parameter | Matrix materials | Sensitivity/ pKa | Dynamic working range/ working range | Detection limit/ response time | Stability | Ref. |
|---|---|---|---|---|---|---|
| Different types of pH indicators including phenol red, bromocresol green, and phenolphthalein, lanthanide complexes, coumarin-based indicators | Different types of matrix materials cellulose acetate, poly(vinyl alcohol), Nafion, ethylcellulose, hydrogels, polyurethane, poly(allylaminehydrochloride), poly(acrylic acid), sol–gel-based materials, ORMOSILS | – | – | – | – | [10] |
| Polypyrrole (PPy) film obtained by chemical oxidation of pyrrole / Absorption based response at 650 nm | Deposited as a thin film on the walls of a polystyrene cuvette | pKa: around 8.6 | Between pH 6 and 12, the | 10–20 s-2 min. | Independent response of ionic strength | [11] |
| Prussian blue *and* *N*-substituted polypyrroles/ modified with enzymes Absorption based response for pH, urea, acetylcholine and peptides | Polystyrene cuvettes | NA | pH in the range of 5–9 | At pH levels greater than 9, irreversible decomposition | Operational stability exceeded 1 month and even after 2 months of dry storage at room temperature | [12] |
| Ruthenium(II)-4,7-dipheny-l-1,10-phenanthroline(Ru(-dpp) ) and fluorescein / time resolved imaging of pH | Poly(acrylonitrile)-based core that contains phosphorescent luminophore $Ru(dpp)_2$ and a hydrogel shell with covalently bound carboxyfluorescein or planar sensor foils | pKa: 7.2 ($n = 12$) RSD between 1 and 2%. | Quantitative mapping of pH gradients between pH 4 and pH 9. Response between pH 5 to pH 8.5 | High-speed screening within one second | NA | [13] |
| 2′,7′-Dichlorofluorescein octadecylester, 2'-Chlorofluorescein Octadecylester 2'-Chloro-7'hexylfluoresc-ein Octadecylester 2′,7′-Dihexylfluorescein octadecylester | Immobilized in proton-permeable hydrogel | p*K*a of 5.5, 6.8, 7.00 and 8.5 | pH 4.5 to 8. | NA | Chromophores of higher lipophilicity: less subject of leaching. The maximum loss in absorption within one week: 5.2% The fluorescein: limited photostability, irreversible photobleaching process, chloro substituent: significantly increase in photostability. | [14] |
| Perylene bisimide (PBI) dyes | Non-covalently entrapped in polyurethane hydrogel and in polyhydroxyalkylmethacrylates | Apparent pKa in PHEMA: 4.9, 4.8 and 6.8 | pH between 3.9–7.8 and 2.9–7.3 | NA | IA/IB decreases from 5.5 to 2.9 within 4 weeks | [15] |
| Covalently linkable rhodamine dyes | Silica gel and cross-linked poly(2 hydroxyethylmethacrylate), (poly(HEMA) beads | $\tau 90 < 2$ min for silica gel, $\tau 90 = 2$–3 min for poly(HEMA) | For silica gel pH 3–8, for poly(HEMA): pH 4–9 | NA | Good response times, repeatability and long-term stability. | [16] |
| A series of coumarin derivatives bearing combinations of amino, dimethylamino, and hydroxyl groups, as well as acetamide and methoxy groups | 3 mM solutions in 10 mM sodium phosphate buffer containing 0.3% DMSO as a co-solvent | pKa: 8.0, 7.2, 9.7 | pH range centered on pH 8–9 | NA | NA | [17] |

**Table 1** (continued)

| Sensitive dye/ measured parameter | Matrix materials | Sensitivity/ pKa | Dynamic working range/ working range | Detection limit/ response time | Stability | Ref. |
|---|---|---|---|---|---|---|
| Condensation product of 5-Hydroxymethyl furfural and rhodamine B hydrazide (RBF)/ fluorescent based sensor, dual response towards pH and copper | Britton–Robinson (BR) buffer | pKa value of 5.02 | pH range from 7.50 to 3.73 | Reversible between pH 7.20 and 4.50 | Stable response in the pH range of 7.00–10.00 | [18] |
| Benzimidazo[2,1-a]benz[de]isoquinoline-7-one-12--carboxylic acid based fluorescent probes dual response towards pH and iron | $H_2O/CH_3CN$ (1/9, v/v) solution | pKa: 3.52 and 6.88 for two different probes | Acidic pH range from 5.80 to 1.80 and alkaline range from 9.10 to 4.50 for two different probes. | Reversible response in the pH ranges of 5.80–1.80 and 9.10–4.50. | NA | [19] |
| Carbazole derivative (9-butyl-bis-3-(4-(dimethylamino) phenyl) allylidene)-9H-carbazole-3,6-diamine) along with silver nanoparticles | Plasticized ethyl cellulose (EC) matrix | The pKa: $4.42 \pm 0.07$ ($n = 3$) and $4.17 \pm 0.08$ ($n = 3$) for emision and absorption based response, respectively. | Good reproducibility for both Ag-free and Ag containing composites. | Reversible response 29 and 27 min. Response+ recovery times for Ag-free and Ag containing composites. | The excellent short term and 16 months of long term stability | [20] |
| Label-free amino modified silicon Nano dots (SiNDs) | Britton- Robinson buffer | NA | pH range of: 2.01–11.02 | Reversible response between pH:3.3–8.8 | Strong fluorescence high photostability | [21] |
| $N^1E,N^2E$)-$N^1,N^2$-bis((-E)-3-(4-(dimethylamino)phenyl)allylidene)ethane-1,2-diamine (SDA), (E)-$N^1$-((E)-3-(4-(dimethylamino)phenyl)allylidene)-$N^4,N^4$-dimethylbenzene-1,4-diamine (SDC) | PMMA and EC | NA | pH 2.00- to pH 12.00 for different compositions | Reversible response between pH:2.00–12.00 | Good response times, repeatability and long-term stability. | This work |

$AgNO_3$ were purchased from Merck. 1-Butyl-3-methylimidazolium tetrafluoroborate was supplied from Fluka.

Acid solutions were prepared with hydrochloric acid and potassium chloride (for around pH: 2.0), disodium hydrogen phosphate/citric acid (for around pH: 5.0), potassium dihydrogen phosphate/sodium hydroxide (for around pH: 7.0), and boric acid ($H_3BO_3$)/ sodium hydroxide / potassium chloride (KCl) for the alkaline pHs in carbon dioxide-free water. Millipore water was used throughout the studies. Solutions of metal cations were prepared from respective metal nitrates, sulphates or chlorides and diluted with $5.0 \times 10^{-3}$ M buffers of demanded pH. The pH values of the solutions were checked using a digital pH meter (Orion) calibrated with original standard buffer solutions. All of the experiments were carried out at room temperature; 20 ± 1 °C. Quinine Sulphate (in 0 .5M $H_2SO_4$; Φ = 0.546) was used as reference dye for the quantum yield calculations of the SDA and SDC. Synthesis of the dyes has been performed following the literature information published earlier by Nesterov et al. [21].

**($N^1$E,$N^2$E)-$N^1$,$N^2$-bis((E)-3-(4-(dimethylamino) phenyl)allylidene) ethane-1,2-diamine (SDA):** $^1$H NMR: SDA: ($CDCl_3$, 400 MHz, d): 2.98 (s, 12H, $NCH_3$); 3.76 (s, 4H, $NCH_2$); 6.6; 7.3 (d, J ¼ 2.3 Hz, 8H, $Me_2N$-$C_6H_4$); 6.7 (dd, J ¼ 4 Hz, 2H, Me2NC6H4-CH]CH); 6.8 (d, J ¼ 4 Hz, 2H, $Me_2NC_6H_4$-CH=CH); 7.96 (d, J ¼ 2.1 Hz, 2H, CH=N). $^{13}$C NMR: SDA ($CDCl_3$,400 MHz, d): 164.55 (CH=N); 151.06; 142.25; 128.78; 112.32 (C aren); 124.44; 124.10 (C=C); 62.10 ($NCH_2$); 40.45 ($NCH_3$). m.p.: SDA: 195–198 °C.

**(E)-$N^1$-((E)-3-(4-(dimethylamino) phenyl)allylidene)-$N^4$,$N^4$-dimethylbenzene-1,4-diamine (SDC):** $^1$H NMR: SDC: ($CDCl_3$, 400 MHz, d): 2.96; 3.00 (s, 12H, $NCH_3$); 6.7 (m, 4H, $Me_2NC_6H_4C$; $Me_2NC_6H_4N$); 6.95 (m, 2H, $Me_2NC_6H_4$eCH] CH); 7.16 (d, J ¼ 2.2 Hz, 2H, $Me_2NC_6H_4N$); 7.38 (d, J¼ 2.2 Hz, $Me_2NC_6H_4C$); 8.25 (d, J¼2 Hz, CH] N).$^{13}$C NMR: SDC: ($CDCI_3$, 400 MHz, d): 157.97 (CH] N); 151.17; 149.36; 128.97; 124.94; 124.65; 122.20; 113.24; 112.36 (C aren); 142.78 (C] C); 41.01; 40.45 ($NCH_3$). m.p.: SDC: 238–240 C°.

Schematic structures of the employed pH probes are shown in Fig. 1.

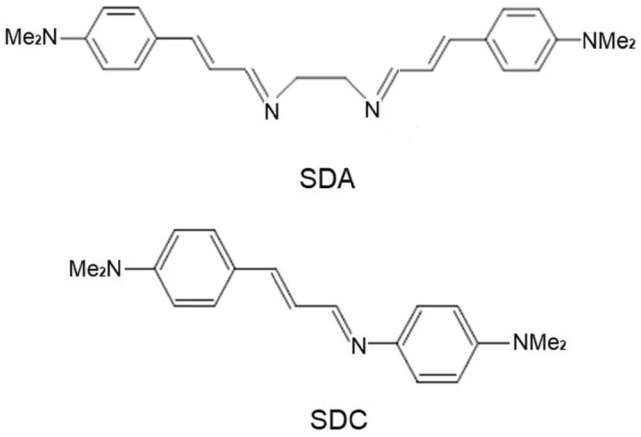


**Fig. 1** Schematic structures of the SDA and SDC dyes

## Instrumentation

Steady-state florescence and lifetime measurements of the pH sensitive dyes were performed by a spectrofluorometer from Edinburg Instruments (FLS920). During lifetime measurements the samples were excited with a xenon lamp or a diode laser and the data were acquired on the principle of time correlated single photon counting (TCSPC). The excitation and emission slits were set to 2.5 nm throughout the measurements. The Instrument Response Function (IRF) tests were performed by water suspension of colloidal silica (LUDOX 30%, from Sigma Aldrich). The decay time data were processed by iterative convolution and the reduced chi-square values were less than 1.2. A programmable syringe pump (Top-5300) and a high voltage power supply (Gamma High Voltage ES30) were used for preparation of the electrospun fibers or mats. The surface morphologies of the fibers and films were controlled using scanning electron microscope (SEM) instrument (FEI QUANTA FEG 250). Size distribution analysis of the AgNPs was performed with a Zeta sizer instrument (Malvern Instruments Ltd.), in dispersed sol form, in water.

## Preparation of Silver Nanoparticles

Silver nanoparticles (AgNPs) were synthesized following the literature information by Solomon [22]. 30 mL of 1.0 mM $AgNO_3$ was added slowly into the 90 mL of 2.0 mM sodium borohydride in an ice bath under continuous stirring. A large excess of sodium borohydride was added to be sure to be reduced all of the ionic silver. Prior to the separation, when the AgNPs were in the sol form, the plasmon resonance of the silver yielded an absorption peak centered at 400 nm which corresponds to the average particle size of 40 nm (See Fig. 2-I and II). Size of the produced AgNPs was also controlled by size distribution analysis approach. The centrifuge (6000 RPM) method at 5 °C was used to separate the silver nanoparticles. After centrifugation at room temperature, we applied two consecutive washing processes with THF. After a 20 min. of sonification, the AgNPs were kept under THF for further studies.

## Preparation of the Electrospun Fibers and Thin Films

Composition of the utilized sensing materials and additives were shown in Table 2. Polymethyl methacrylate (PMMA) ethyl cellulose (EC) and other additives along with indicator dyes were dissolved in tetrahydrofuran, in 25 mL of glass vials. All of the constituents were mixed under magnetic stirring. The resulting transparent and

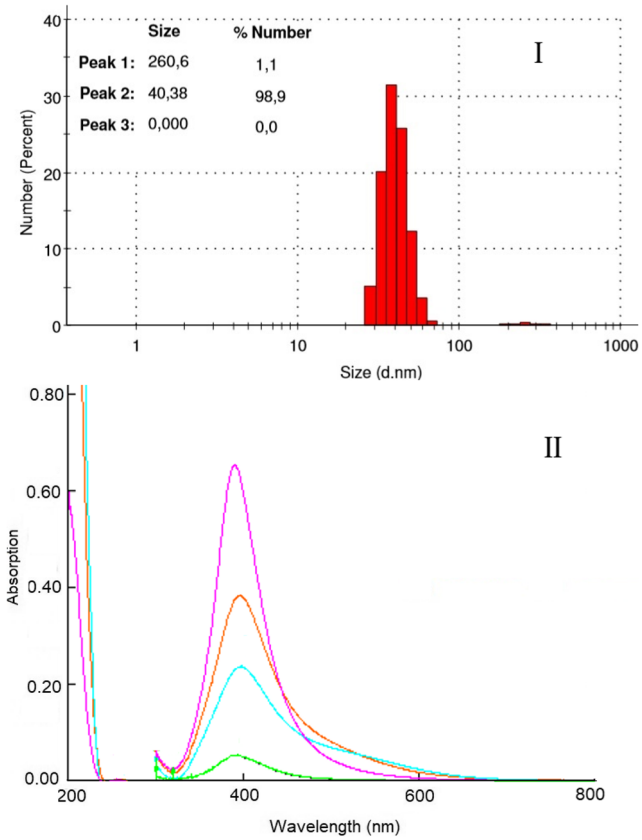


**Fig. 2** I: Size distribution analysis results of AgNPs II: Absorption spectra of different concentrations of AgANPs in form of yellow sol

homogeneous mixture was spread onto a polyester support (125 μm, Mylar TM type) by knife coating technique or exposed to high voltage for the electrospinning procedure. The ionic liquid or silver doped formulations exhibited better response and excellent spinning ability under high voltage with respect to the additive-free ones. Therefore, in the further studies we utilized the IL and silver doped forms, intensively. In order to perform the electrospinning, the homogeneous composite was placed in a 10 mL plastic syringe equipped with a 21G: 0.80 × 38 mm metallic needle. The syringe was placed on the programmable syringe pump and the electrodes of the high voltage power supply were clamped on the metallic needle and the aluminum substrate. The feed rate of the composite and the applied voltage were 2.0 mL/h and 26 kV, respectively. The electrospun fibers or mats were deposited on the surface of the aluminum substrate.

The SEM images of the electrospun materials under various magnifications were shown in Fig. 3. Both, the Ag-free and Ag-doped electrospun materials made up of PMMA or EC, exhibited similar porous structures. Usage of the PMMA resulted with formation of more fiber-like structures. Presence of the AgNPs in the matrix, enhanced formation of fibers in the PMMA (See Fig. 3c and d ). This type of fibrous-structure of the electrospun membrane provides higher surface area with respect to the continuous thin films.

## Acid Induced Studies and Immunity Tests

In this work, the acid-base sensitivity tests of the pH probes were performed in two different ways. The acidity constants of the immobilized SDA and SDC have been calculated after exposure to certain concentrations of the buffer solutions in the pH range of the 2.50–12.00. The thin film or fiber forms of the test materials were immersed into the buffer solutions until

**Table 2** Composition of the exploited sensing agents

| Matrix(mg) | Additives | | | | |
|---|---|---|---|---|---|
| | Ionic liquid (mg) | Plasticizer (DOP) (mg) | potassium tetrakis-(4-chlorophenyl) borate (mg) | AgNPs (mg) | Dye |
| PMMA(240 mg) | 48 | 192 | 5 | – | 2 mg SDA |
| PMMA(240 mg) | – | 192 | 5 | – | 2 mg SDA |
| PMMA(240 mg) | 48 | 192 | 5 | 2 | 2 mg SDA |
| EC(240 mg) | 48 | 192 | 5 | – | 2 mg SDA |
| EC(240 mg) | – | 192 | 5 | – | 2 mg SDA |
| EC(240 mg) | 48 | 192 | 5 | 2 | 2 mg SDA |
| PMMA(240 mg) | 48 | 192 | 5 | – | 2 mg SDC |
| PMMA(240 mg) | – | 192 | 5 | – | 2 mg SDC |
| PMMA(240 mg) | 48 | 192 | 5 | 2 | 2 mg SDC |
| EC(240 mg) | 48 | 192 | 5 | – | 2 mg SDC |
| EC(240 mg) | – | 192 | 5 | – | 2 mg SDC |
| EC(240 mg) | 48 | 192 | 5 | 2 | 2 mg SDC |

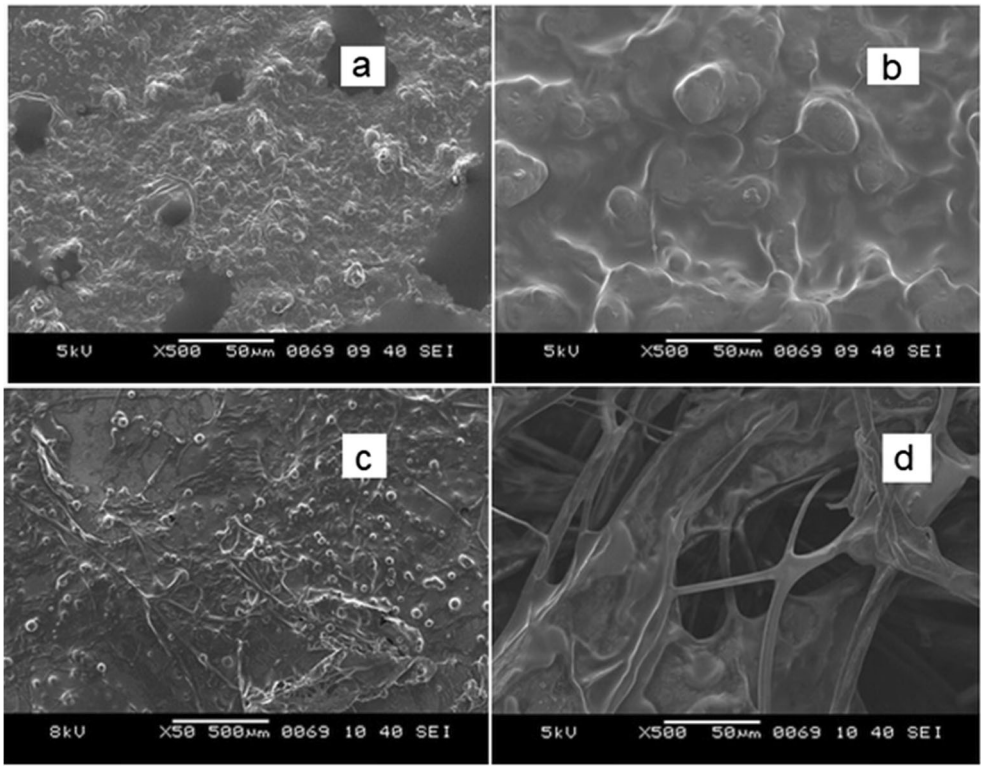


**Fig. 3** SEM images of SDA containing electrospun materials under ×500 magnification a: Ag free, b: Ag doped EC based mats; c: Ag free, d: Ag doped PMMA based materials

the equilibrium reached and spectral response were recorded for each pH value. The acidity constants were calculated by using non-linear fitting algorithm of Gauss–Newton–Marquardt method (See Eq. 1) [23].

$$\mathrm{pKa} = pH + log\frac{(Ix-Ib)}{(Ia-Ix)} \quad (1)$$

where $I_a$ and $I_b$ are emission intensities of acidic and basic forms and $Ix$ is the emission at a pH near to the p$K$a. Table 3 reveals the acidity constants of the Ag-free and Ag-doped thin films or electrospun mats of the SDA and SDC, respectively. The second group tests were performed after exposure to high concentrations of strong acid vapors of the same test material in a closed desiccator. This group of tests were named as "acid immunity tests" We exposed the sensor slides to the different concentrations of acid vapors in a closed desiccator with an internal volume 5 L by placing 40 mL of acid (contained in the 50 mL beaker). The vapors were obtained by evaporation of different acids at room temperature. The mean laboratory temperature was 20 °C (±0 .7°C) throughout the experiments. Concentrations of the acid vapors were calculated using their partial vapor pressure at 20 °C (HCl: 10.6 mmHg, $H_2SO_4$: 36 mmHg and $HNO_3$: 48 mmHg). The partial pressures were also converted to percent composition (% *v*/v) for all of the acids and were found to be 1.39, 4.73 and 6.32% (v/v in air) for the HCl, $H_2SO_4$ and $HNO_3$, respectively.

## Results and Discussion

### Spectral Properties of the Dyes

Chemical structures of the utilized pH probes were shown in Fig. 1. Absorption, excitation and emission spectra of the SDA and SDC, were recorded in the solvents and in the polymeric matrices of EC and PMMA. The UV-vis spectroscopy related data of the dyes were shown in Table S1. The SDA and SDC exhibited efficient absorbance and high molar extinction coefficients around 400 nm in all of the test moieties. Fig. S1 and S2 reveal large absorption bands extending from 330 to 545 nm and from 320 to 600 nm for the SDA and SDC, respectively. The excellent absorption abilities of the dyes make their excitation possible for a large spectral range. However, herein we have chosen the 390 nm as the excitation wavelength where both the AgNPs and the dyes can be excited at the same time. Absorption maxima, intensities and molar extinction coefficients of the dyes exhibited significant variations when embedded in polymeric matrices along with the ionic liquid and/or AgNPs. Figure 4 reveals excitation-emission spectra of the SDA in THF, EC and PMMA, respectively. The SDA exhibited red shift both in the excitation and emission wavelength when embedded in the solid matrices. The emission maxima of the SDA exhibited 65 nm of red shift (from 468 to 533 nm) from the THF to the EC. In the PMMA, the emission

**Table 3** Acidity constants of the SDA and SDC before and after exposure to high concentrations of strong acid vapors

| **SDA** | | **pKa (acid-free)** | **pKa (after acid-exposure)** |
|---|---|---|---|
| Thin Film | Ag- free | $pKa_1 = 5.00$<br>$pKa_2 = 11.22$ | – |
| Thin Film | Ag- doped | $pKa_1 = 5.56$<br>$pKa_2 = 10.75$ | – |
| Electrospun mats | Ag- free | $pKa_1 = 5.93$<br>$pKa_2 = 11.76$ | – |
| Electrospun mats | Ag- doped | $pKa_1 = 5.54$<br>$pKa_2 = 11.60$ | – |
| Electrospun mats | Ag- free | – | HCl/<br>$pKa_1 = 3.25$<br>$pKa_2 = 6.57$ |
| Electrospun mats | Ag- doped | – | HCl/<br>$pKa_1 = 3.80$<br>$pKa_2 = 7.65$ |
| Electrospun mats | Ag- free | – | $HNO_3$/<br>$pKa_1 = 7.35$<br>$pKa_2 = -$ |
| Electrospun mats | Ag- doped | – | $HNO_3$/<br>$pKa_1 = 6.30$<br>$pKa_2 = -$ |
| **SDC** | | **pKa (acid-free)** | **pKa (after acid-exposure)** |
| Electrospun mats | Ag- free | $pKa_1 = 7.05$<br>$pKa_2 = -$ | – |
| Electrospun mats | Ag- doped | $pKa_1 = 7.93$<br>$pKa_2 = -$ | – |
| Electrospun mats | Ag- free | – | $H_2SO_4$/<br>$pKa_1 = 8.56$<br>$pKa_2 = -$ |
| Electrospun mats | Ag-doped | – | $H_2SO_4$/<br>$pKa_1 = 7.22$<br>$pKa_2 = -$ |

maximum appeared at 10 nm further wavelength with respect to the EC exhibiting a red shift of 75 nm (See Fig. 4-I). Figure 4-II reveals spectral behavior of the thin film and electrospun fibers of the Ag-free and Ag- doped sensing materials. Spectral shifts extending to 10 nm were observed due to the structural changes of the matrix or the chemical variations arising from the dopant. However, in both forms, presence of the AgNPs within the matrix resulted with enhanced emission with respect to the Ag-free formulations.

The excitation and emission spectral data of the all of the sensing composites were recorded both in the absence and presence of the IL. The IL provided extra stability for the dyes due to the buffer-like chemical behavior which will be explained into detail in further paragraphs. Therefore, further studies were completely performed in the IL doped moieties. Table 4 reveals emission based spectral characteristics of the SDA and SDC in all of the matrices for the Ag-free and Ag-doped forms in terms of the excitation and emission wavelength, Stoke's shift and quantum yield. Excitation maxima of the SDA appeared at 388, 487 and 499 nm in the THF, EC and PMMA, respectively. As reported earlier, the pH probes contain available active centers for proton attacks and may be named as Schiff bases [20]. The dyes display intramolecular charge transfer in the excited state since the N,N-dimethylamino moiety is a more effective electron donating group with respect to the central nitrogen atoms of N1 and N2. Therefore, pH sensitivity of the symmetric Schiff base of SDA can be attributed to the successive protonation of the nitrogen atoms of N1 and N2. The protonation of the excited states of the dyes results in an increase in the luminescence intensity in low pH solutions. Similarly, the acid-base chemistry of the non-symmetric Schiff base, SDC can be assigned to the stepwise protonation of the nitrogen moiety. In both cases, at low pHs, protons are reversibly extracted

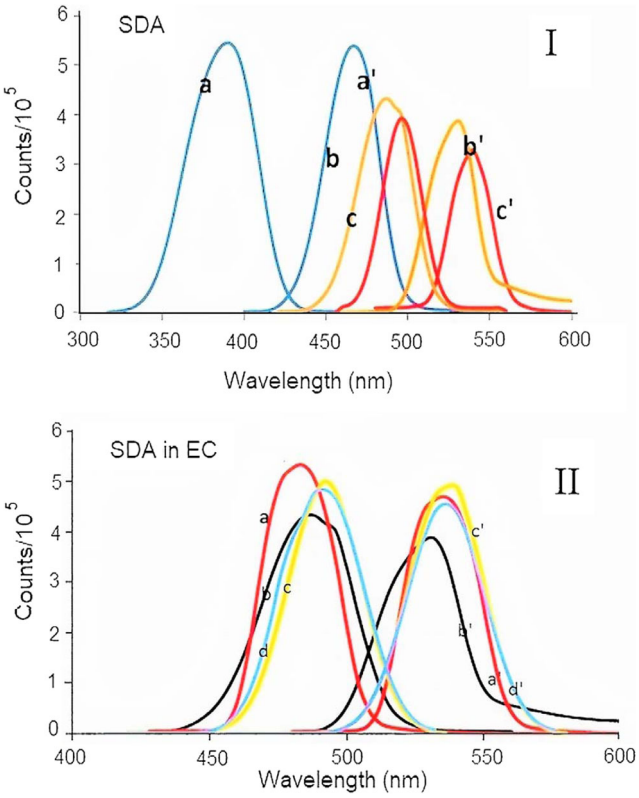


**Fig. 4** The excitation-emission spectra of the SDA I: a, a': in THF; b, b': in EC and c, c': in PMMA. II: The excitation-emission spectra of the EC doped SDA a, a': Ag-doped thin film; b, b': Ag-free thin film; c, c':Ag-doped fiber; d, d': Ag-free fiber

into the EC or PMMA membranes by the lipophilic anionic additive as had been explained in the published work of Wolfbeis et al. [24].

## Interaction of the AgNPs, Dyes and the Proton

In the present work interaction between the pH probes and the AgNPs resulted with an unexpected enhancement in the emission based pH sensing ability of the dyes. In order to clarify the mechanism behind this enhancement, steady-state and time domain fluorescence measurements were carried out for the solely AgNPs and dyes, and for the Ag-doped dyes in the EC matrix, respectively.

## Interaction of AgNPs with Proton

In colloids, AgNPs exhibit strong colors arising from electron oscillations induced by incident light, which is referred to as the plasmon absorption. We measured a strong emission band in water dispersed yellow sols at 450 nm when excited at 390 nm (See Supporting info, Fig. S3.). The AgNPs exhibited a narrow Plasmon peak with an effective bandwidth of 19 nm. However, when embedded in the EC matrix along with other additives, both the excitation and emission bands are broadened, splitted and blue shifted with respect to the sol form. The splitted excitation and emission peaks appeared at 316 and 392, and, 450 and 504 nm, respectively. When the AgNPs are exposed to highly acidic conditions, both the excitation and emission spectra exhibited significant blue shift and difference in shape. Figure 5 reveals normalized steady-state excitation and emission spectra of the EC doped AgNPs under neutral and acidic

**Table 4** Emission based spectral characteristics of the Ag-free and Ag doped forms of the SDA and SDC in terms of excitation wavelength ($\lambda_{ex}$), emission wavelength ($\lambda_{em}$), Stoke's shift ($\Delta\lambda$) and Φf: quantum yield. TF: thin film, NF: nano fiber

| Dye | Matrix | Thin film/ nanofiber | AgNPs (2 mg) | $\lambda_{max}^{ex}$(nm) | $\lambda_{max}^{em}$(nm) | Stoke's shift ($\Delta\lambda$) (nm) | Quantum yield ($\Phi_F$) |
|---|---|---|---|---|---|---|---|
| SDA | THF | _ | _ | 388 | 468 | 80 | 0.361 |
| SDA | EC | TF | _ | 484 | 532 | 48 | 0.420 |
| SDA | EC | TF | + | 487 | 533 | 46 | 0.191 |
| SDA | EC | NF | _ | 490 | 535 | 45 | _ |
| SDA | EC | NF | + | 492 | 538 | 46 | _ |
| SDA | PMMA | TF | _ | 496 | 540 | 44 | _ |
| SDA | PMMA | TF | + | 495 | 542 | 47 | _ |
| SDA | PMMA | NF | _ | 499 | 543 | 44 | _ |
| SDC | THF | _ | _ | 422 | 478 | 56 | 0.431 |
| SDC | EC | TF | _ | 594 | 651 | 57 | 0.501 |
| SDC | EC | TF | + | 598 | 656 | 58 | 0.278 |
| SDC | EC | NF | _ | 598 | 655 | 57 | |
| SDC | EC | NF | + | 604 | 656 | 52 | |
| SDC | PMMA | TF | _ | 606 | 654 | 48 | |
| SDC | PMMA | TF | + | 608 | 657 | 49 | |
| SDC | PMMA | NF | _ | 610 | 655 | 45 | |
| SDC | PMMA | NF | + | 613 | 660 | 47 | |

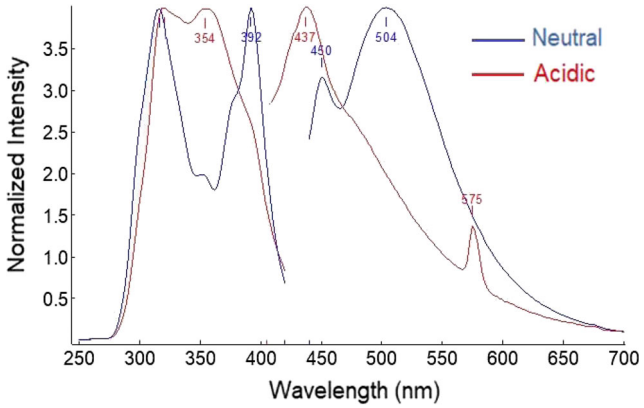


**Fig. 5** Normalized excitation and emission spectra of the AgNPs in EC under neutral and acidic conditions (pH = 7.1 and pH = 2.3 acidified with HCl)

conditions, respectively. The spectral patterns observed in the alkaline form were nearly same of the neutral form. From Fig. 5 it can be concluded that presence of the protons in the test moiety has a distinct effect on the spectral characteristics of the embedded AgNPs. Since the tests had been performed with a HCl solution, the spectral shifts cannot be attributed to the oxidation of the metallic silver atoms. Penetration of the proton into the membrane by the ion exchange causes quenching of the emission band observed at 504 nm indicating presence of an interaction between the proton and collective oscillations of the electron gas of excited plasmons.

## Interaction of the SDA and SDC with the Acids

The reaction between the utilized Shciff-bases of SDA and SDC and proton is a convenient protonation-deprotonation type of interaction. As explained earlier, the Schiff bases become reversibly working proton sensitive probes when embedded in the EC along with the potassium tetrakis-(4-chlorophenyl) borate [20]. They may be tailored in form of thin films or electrospun fibers. In these systems, $H^+$ ions are extracted into the polymeric phase, attack towards the proton active centers, meanwhile potassium ions diffuse from the membrane into the aqueous phase according to the mechanism of ion-exchange. Following these successive and fast protonation steps, color of the embedded dyes turns from pale red to orange and from yellow to dark purple for the SDA and SDC, respectively. As a result, both the AgNPs and the dyes are effective to response the pH. However, when they are used together, they exhibit enhanced, repeatable and reversible signal towards proton even in harsh conditions like the work-places saturated with the acid vapors. On the other hand, acidity constant is an indicator of the pH sensitivity of a fluorescent probe. Herein both, the SDA and SDC exhibited distinct emission based pH induced response for a quite large range of the pH scale extending from 2.50 to 12.00. While the SDA exhibiting two different acidity constants centered around 5.50 and 11.50, the SDC exhibited a sensitivity towards proton around pH 7.50.

## Why Do the SDA and SDC Work more Effective along with the AgNPs?

When the pH probes and the AgNPs are used together, pH sensing ability of the dyes enhanced distinctly. Mechanism of the interaction between the fluorescent probes and silver nanoparticles has been determined from steady-state and lifetime based measurements. First of all, the possibility of a spectral overlap between donor and acceptor has been evaluated.

Figure 6 I and II reveal gathered excitation and emission spectra of the SDA/AgNPs and SDC/AgNPs, respectively. According to Fig. 6-I, both the excitation and emission spectra of the SDA overlaps with the excitation and emission bands of the AgNPs, when excited at the 390 nm. However, there is a limited overlap between the emission band of the AgNPs and the excitation band of the SDA. This limited overlap comparatively enhances the emission based response of the SDA. However, in case of the SDC, emission band of the AgNPs completely overlaps with the excitation band of the SDC which means an energy transfer from the AgNPs to the SDC (See Fig. 6-II). These features make the AgNPs excellent potential energy transmitter agents that allow us to use the plasmons along with the pH sensitive dyes in the polymeric matrix for pH sensing efforts in a different way. One approach of measuring fluorescence resonance energy transfer (FRET) is

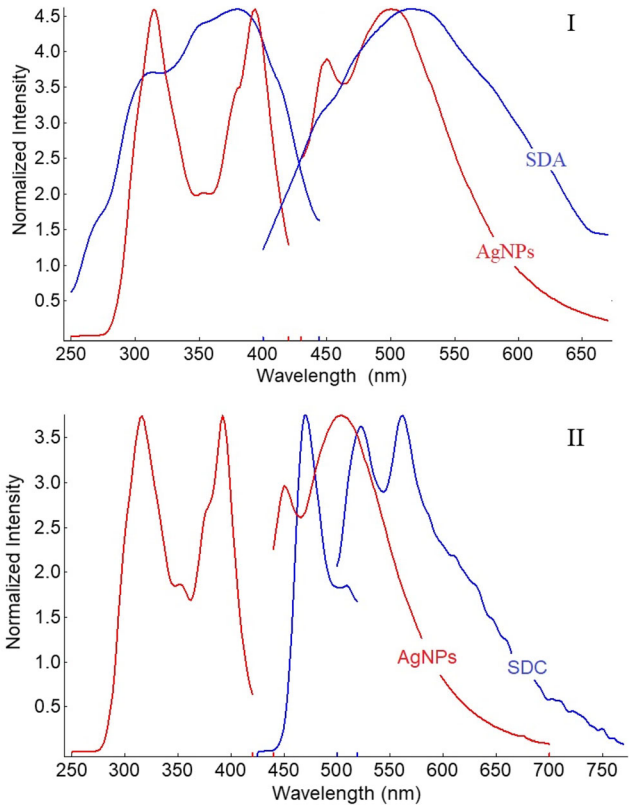


**Fig. 6** Gathered excitation-emission spectra of the **(I)** SDA and AgNPs **(II)** SDC and AgNPs when embedded in EC matrix

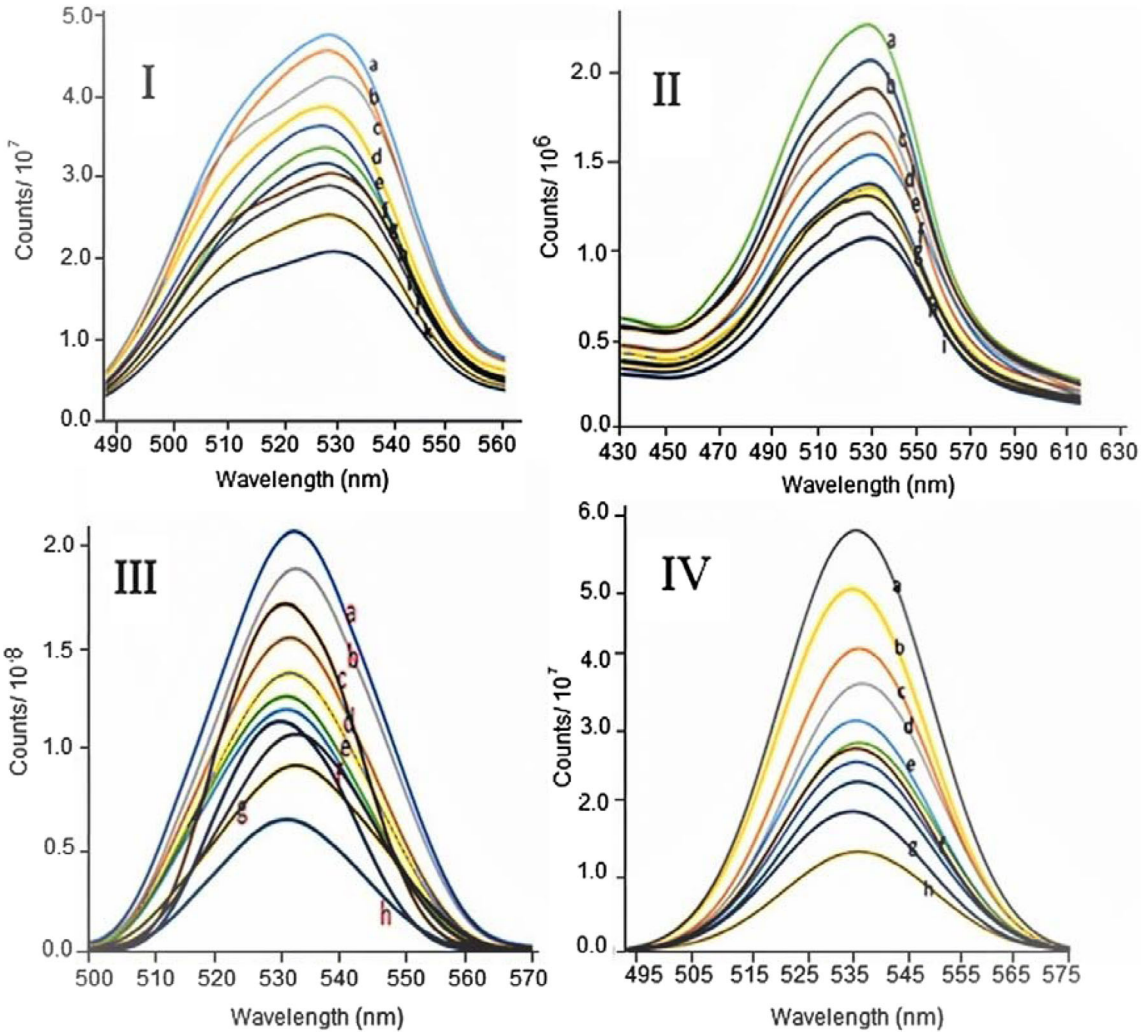


**Fig. 7** The acid induced relative signal changes for the Ag-free and Ag-doped thin films and electrospun fibers of the SDA in the pH range of 3.00–12.00. (I) Thin Film, (II) Thin films doped with AgNPs, (III) Electrospun fiber, (IV) Electrospun fibers doped with AgNPs at pH: (a): 3.00, (b): 4.44, (c): 5.43, (d): 6.48, (e): 7.30, (f): 8.56, (g): 10.25, (h): 10.75, (i): 11.25, (j): 12.00

to record the variation of the emission intensity of the acceptor with varying amounts of the donor. Herein, we recorded emission intensities of the SDA and SDC (acceptors) versus increasing amounts of the AgNPs. In both cases, we observed an enhancement in the emission intensity of the dyes with increasing amounts of the AgNPs up to a critical concentration (2 mg AgNPs/kg polymer). However, after this critical value, the fluorescence intensity of the dyes decreased due to self-quenching

### Lifetime Based Measurements

Lifetime measurements also give us valuable information about on the mechanism of interaction between the fluorophores and silver nanoparticles. The room temperature time resolved fluorescence measurements of the EC embedded AgNPs, SDA, SDA/AgNPs, SDC and SDC/AgNPs were also carried out. The dyes were excited with a laser light source at 367 nm and the emissions were acquired at 504, 532 and 650 nm, for the AgNPs, SDA and SDC, respectively (Laser with 250 p second pulse width).

According to the theory, the lifetime of the donor (AgNPs) will decrease in the presence of the acceptor. Herein we measured lifetime of the EC embedded AgNPs and AgNPs / SDA pair as 10.03 and 1.25 ns, respectively. Similarly, the AgNPs / SDC pair exhibited a decay time of 1.27 ns. These findings can be concluded as another evidence of the FRET from the AgNPs to the dyes.

## Effect of Ionic Liquid on the pH Probes

Herein, we used room temperature ionic liquid (RTIL); 1-Butyl-3-methylimidazolium tetrafluoroborate to enhance the long term stability of the fluorophores. The RTIL containing EC matrix provides an immunity and spectroscopically available microenvironment for the SDA and SDC. Probably, weak

Lewis acid–base interactions taking place between the acidic impurities and the anionic tetrafluoroborate counterpart of the RTIL protects the dye [25, 26]. The excellent short term and 18 months of long term stability can be attributed to the presence of $EMIMBF_4$ within the matrix.

## pH Induced Studies

pH induced response of the test materials have been investigated both, under normal conditions and after exposure of the test materials to the vapors of the strong acids of HCl, $HNO_3$ and $H_2SO_4$. Responses of the SDA and SDC towards acidity were tested between pH 2.50 and 12.00 in the PMMA and EC matrices. The tests were performed for the thin films and electrospun fibers as well as the Ag-free and Ag-doped forms. In all cases the pH probes exhibited better response towards pH when doped in the EC matrix. Therefore, we used the EC as matrix material in the further studies.

The thin film forms of the SDA exhibited a decreasing spectral response in signal intensity from acidic to alkaline pH values at 532 nm when excited at 390 nm. Similar spectral behavior was observed for the nano-fibers at 535 nm. Figure 7 reveals pH induced response of the Ag-free and Ag-doped thin films and electrospun fibers of the SDA in the pH range of 2.50–12.00. All of the test materials exhibited similar and non-sigmoidal response for the studied pH range. The electrospun fibers exhibited better response with respect to the thin films, towards pH. When doped with the AgNPs, while the thin films exhibiting an increase in acid induced relative signal changes from 64 to 78% (See Fig. 7 I and III) the Ag-doped electrospun mats exhibited an enhancement from 63 to 89% (Fig. 7 II and IV).

The SDC exhibited similar pH induced response to the SDA when immobilized in the EC matrix. The emission maxima appeared at; 655 and 656 nm for the Ag-free and Ag doped forms, respectively. Figure 8 reveals pH induced response of the SDC in form of the electrospun mats between pH 3.00–12.00. The pH dependent relative signal change was enhanced from 58 to 79% in the Ag-doped forms (See Fig. 8-I and II).

We also investigated effect of the variation of pH on the decay times of the dye. The pH induced decay plots of the thin film and electropun forms of the dyes in different pH buffers mainly exhibited mono exponential decay behavior and

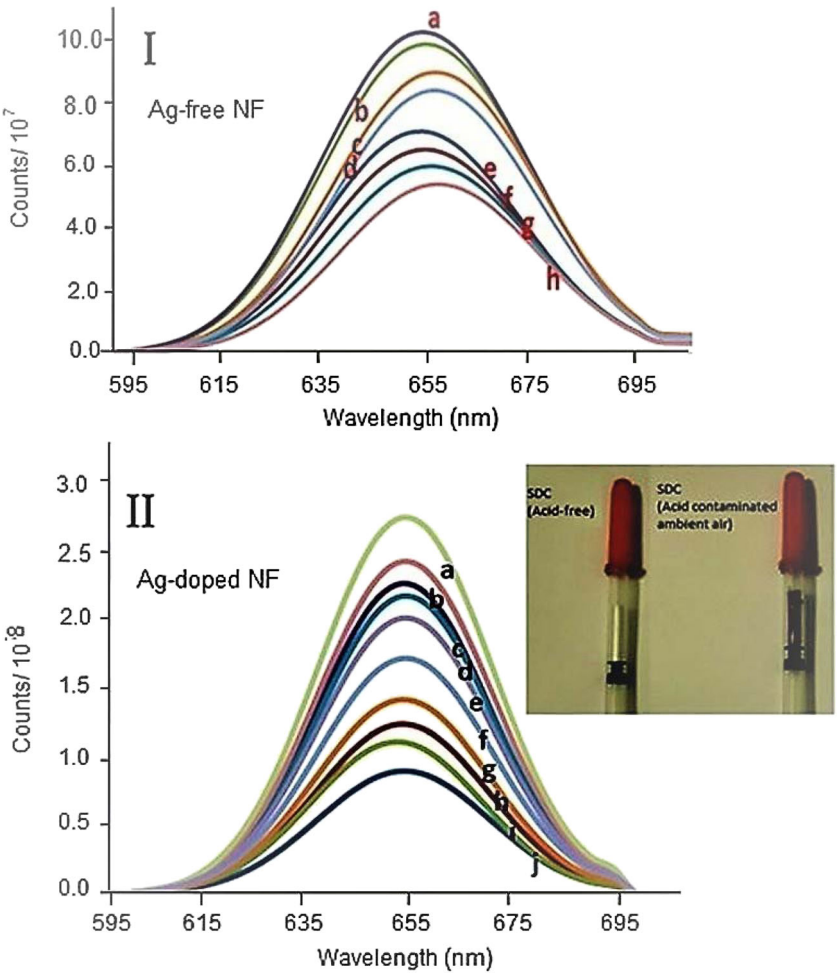


**Fig. 8** pH induced response of the SDC in form of the electrospun mats I: Ag-free, II: Ag doped forms. I: (a): pH: 3.00, (b): 4.44, (c): 5.43, (d): 6.80, (e): 7.30, (f): 8.56, (g): 9,50, (h): 10.25. II: (a): pH: 3.00, (b): 4.44, (c): 5.43, (d): 6.48, (e): 7.30, (f): 8.56, (g): 10.25, (h): 10.75, (i): 11.25, (j): 12.00

yielded slightly different decay times for the acidic, neutral and alkaline moieties (pH = 3.00, 7.00 and 12.00.). Table 5 reveals variation of the decay times in different buffers. Therefore, we did not use the decay times as a calibration tool for the further studies of the SDA and SDC dyes.

## pH Induced Studies after Exposure to Vapors of Strong Acids

pH sensing abilities of the SDA and SDC were also tested with the calibration buffers after exposure of the test materials to vapors of very strong acids of HCl, $HNO_3$ and $H_2SO_4$ to simulate harsh conditions like industrial plants. This group of pH sensitivity tests named as "acid immunity tests". Concentrations of the acid vapors were calculated considering their vapor pressures at 20 °C (HCl: 10.6 mmHg, $H_2SO_4$: 36 mmHg and $HNO_3$: 48 mmHg) which corresponds to the partial pressures of 1.39, 4.73 and 6.32% in the air for the HCl, $H_2SO_4$ and $HNO_3$, respectively. The pH induced response of the poisoned sensing materials was checked with steady-state spectrofluorometric measurements. The acid induced responses of the SDA and SDC based electrospun mats were shown in Figs. 9, 10 and 11. All of the tests were performed both in the absence and presence of AgNPs. Figure 9 -I and II reveal pH sensing performance of the Ag-free and Ag-doped SDA after exposure to HCl vapors.

Similar tests were also performed for the more aggressive oxidizing acids of $H_2SO_4$ and $HNO_3$, respectively. Due to the higher vapor pressures, presence of the $H_2SO_4$ and $HNO_3$ resulted with higher acid concentrations (4.73 and 6.32%) with respect to the HCl in the test moieties. Figure 10 reveals acid sensitivity of the SDA after exposure to the nitric acid for both, Ag-free and Ag doped electrospun fibers.

Spectral results observed for the $H_2SO_4$ were similar to $HNO_3$ but lower in terms of the relative signal drops with respect to the results of the nitric acid. Same tests were applied for the SDC doped materials. Emission based pH sensitivity of the Ag-doped electrospun mats were shown in Fig. 11-I and II which reveals effect of sulphiric acid exposure on the SDC for both Ag-free and Ag-doped forms in a comparative manner. In all cases we observed at distinct immunity against poisoning effect of the acids on the emission ability of the SDA and SDC for the Ag doped forms. Presence of AgNPs within the transparent EC matrix resulted with enhanced luminescence, better resolution and higher relative signal change on the pH sensitivity of the test materials.

**Table 5** The pH induced decay times of the thin film and electropun mats of the AgNPs, dyes and Dye/AgNp pairs in the acidic, neutral and alkaline moieties (pH = 3.00, 7.00 and 12.00)

| Dye | Matrix | Thin film/ nanofiber | AgNPs (2 mg/kg Polymer) | Decay Time (ns) |
|---|---|---|---|---|
| AgNPs | EC | TF | + | 1.86 ± 0.11 (48.2%)17.76 ± 1.16(51.8%) |
| SDA | EC | TF | _ | pH = 12.00, 1.06 |
| | | | | pH = 7.00, 1.13 |
| | | | | pH = 3.00, 1.17 |
| SDA | EC | TF | + | pH = 12.00, 1.24 |
| | | | | pH = 7.00, 1.25 |
| | | | | pH = 3.00, 1.26 |
| SDA | EC | NF | _ | pH = 12.00, 2.11 |
| | | | | pH = 7.00, 1.31 |
| | | | | pH = 3.00, 1.27 |
| SDA | EC | NF | + | pH = 12.00, 1.53 |
| | | | | pH = 7.00, 1.42 |
| | | | | pH = 3.00, 1.20 |
| SDC | EC | TF | _ | pH = 12.00, 1.27 |
| | | | | pH = 7.00, 1.25 |
| | | | | pH = 3.00, 1.23 |
| SDC | EC | TF | + | pH = 12.00, 1.26 |
| | | | | pH = 7.00, 1.27 |
| | | | | pH = 3.00, 1.32 |
| SDC | EC | NF | _ | pH = 12.00, 3.11 |
| | | | | pH = 7.00, 1.58 |
| | | | | pH = 3.00, 0.65 |
| SDC | EC | NF | + | pH = 12.00, 0.58(61.8%), 4.39 (38.2%) |
| | | | | pH = 7.00, 0.50(76.1%), 3.002(23.9%) |
| | | | | pH = 3.00, 0.38(55.6%), 2.00(44.4%) |

## Response and Regeneration Performance of the EC Doped Dyes in Form of Nanofibers

Response and regeneration performance of EC doped dyes were tested with a variety of buffer solutions between pH 2.00–12.00. Kinetic data were acquired with fiber optic probe which is in contact with a flow system. During fiber optic measurements the fluorescence intensity was monitored and recorded versus time. pH determinations were carried out pumping buffer solutions of desired pH. Each buffer solution was pumped for 2 min at a flow rate of 2.2 mL $min^{-1}$. The tests were performed with both thin films and electrospun fibers fixed into a 350 μL homemade flow-cell. Structure of the experimental setup was published in our previous work [23]. Both of the sensing materials responded reversibly towards pH. However, in both cases a signal drift of approximately 10–17.5% was observed after 3rd cycle. The regeneration performance of the tightly fixed thin films was better than that of the nanofiber forms. The observed signal drifts can be attributed to the fluctuations in the flow system. Fixation of nanofibers in the flow cell or to study in lower flow rates may result in better regeneration performance.

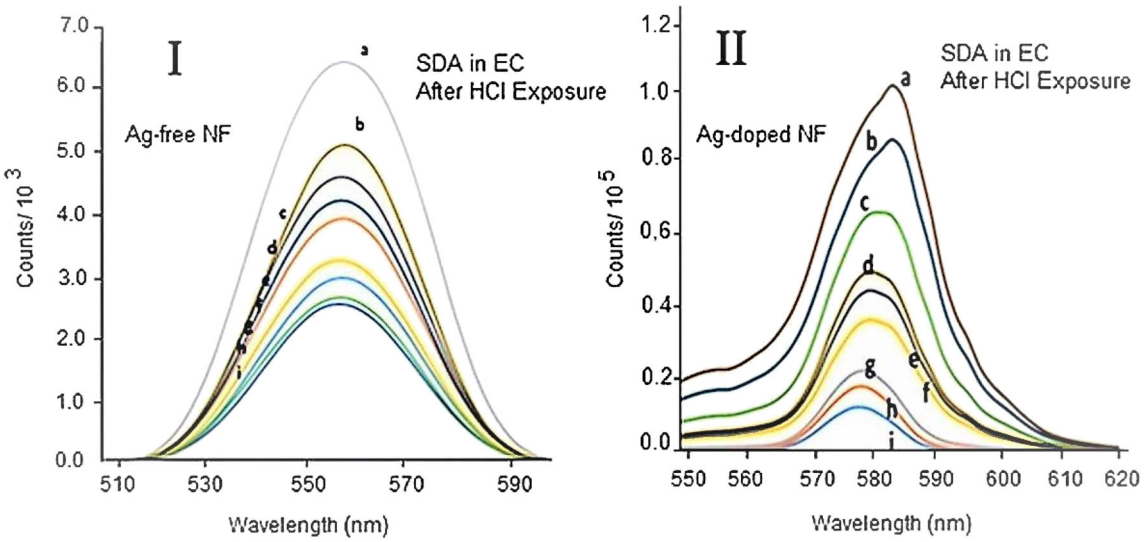


**Fig. 9** I: pH sensitivity of the of the SDA (in fiber form) in EC matrix after exposure to HCl vapors (1.39% *v*/v in air), I:(Ag-free) $\lambda_{ex}$:380 nm $\lambda_{max}$:563 nm, pH: a:2.00; b:3.00; c:4.00; d:5.00; e:6.00; f:7.00; g:8.00; h:9.00; i:10.00. II:(Ag doped) $\lambda_{ex}$:380 nm $\lambda_{max}$:574 nm, pH: a:2.00; b:3.00; c:4.00; d:5.00; e:6.00; f:7.00; g:8.00; h:9.00; i:10.00

## Calibration Plots and pH Detection in Real Water Samples

pH-induced calibration curves of the SDA and SDC has been drown using the spectral data given in Fig. 7-IV and Fig. 8 –II, for the pH range of 2.50–12.00 and 3.00–12.00 respectively. The derived plots were shown in Fig. 12-I and –II. Herein we used the intensity ratio of (I-I0)/I0 which gives good straight lines over the working range. In spite of the applied algorithm, both, the SDA and SDC exhibited non-linear spectral response described by $y = -0.0018 \times ^{3} + 0.0443 \times ^{2} - 0.3864x + 0{,}703$ ($R^2 = 0.9926$) and $y = -0.0006 \times ^{3} + 0.0107 \times ^{2} - 0.1229x + 0.2823$ ($R^2 = 0.9976$) towards pH for the pH range extending from 2.50 to 12.00. However, both the SDA and SDC exhibited more linear spectral response and reasonable $R^2$ values between pH = 2.50–7.20 and 3.00–8.56 (See inset of Fig. 12-I and II).

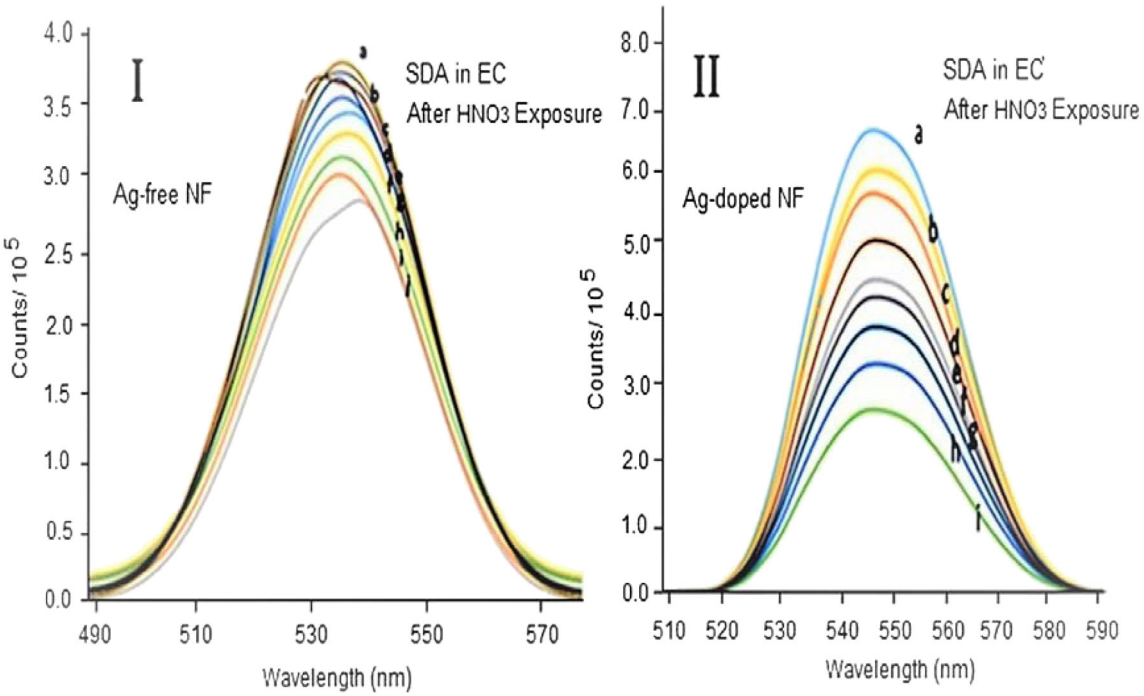


**Fig. 10** pH sensitivity of the of the SDA (in fiber form) in EC matrix after exposure to $HNO_3$ vapors I: (Ag-free) $\lambda_{ex}$:370 nm $\lambda_{max}$: 533 nm, pH: a: 2.50; b:3.00; c:4.44; d:5.56; e:6.30; f:7.20; g:8.56; h:9.58; i:10.25; j:11.75. II: (Ag-doped) λex:370 nm, λmax: 552 nm, pH: a: 2.50; b:3.00; c:4.44; d:5.56; e:6.30; f:7.20; g: 8.56; h:9.58; i:10.25; j:11.75

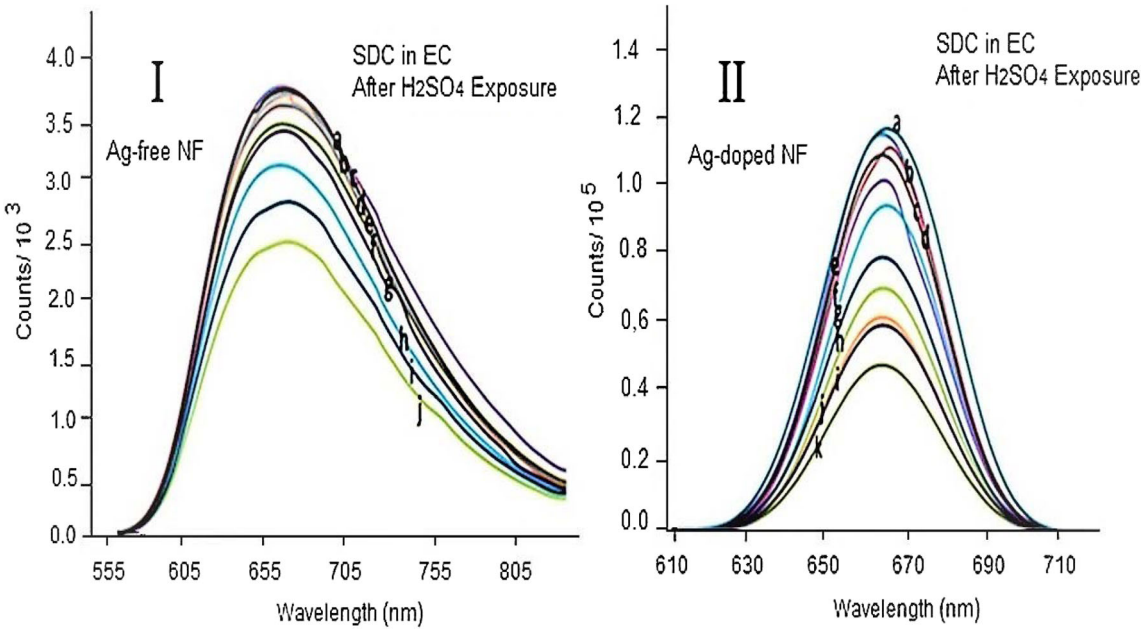


**Fig. 11** I: pH induced emission characteristics of SDC in fiber form in EC matrix after exposure to $H_2SO_4$ vapors (4.73%). %) I: (Ag free) $\lambda_{ex}$:385 nm, $\lambda_{max}^{em}$: 668 nm, pH: a: 2.50; b:3.00; c:4.44; d:5.56; e:6.30; f:7.20; g:8.56; h:9.58; i:10.25; j:11.75 II: (Ag doped) $\lambda_{ex}$:385 nm $\lambda_{max}^{em}$: 663 nm, pH: (a): 2.30; (b): 3.00; (c): 3.50; (d): 4.44; (e): 5.43; (f): 6.80; (g): 7.30; (h): 8.56; (i): 9.58; (j): 10.75; (k): 11.75

To evaluate feasibility of the offered pH probes for the detection of acidity, filtered and acidified real tap water samples spiked with different concentrations of hydrochloric acid were used. The samples provided from the campus of University of Dokuz Eylul were pre-treated by qualitative filter paper and 0.45 μm filter membrane to remove the solid suspensions and other impurities. The pH values of the acidified tap water samples were measured utilizing a pre-calibrated pH meter equipped with a glass electrode and with the SDA and SDC, respectively. Prior to the pH measuerents, three point calibration of the instrument (Orion Star A211) using automatic buffer recognition of NIST has been performed. The tap water samples were spiked with the 10, 50, 100, 150, 200 and 300 μL of $10^{-3}$ M of HCl solutions in 2.5 mL of sample cuvettes. Three replicate measurements were performed for each sample. Table 6 reveals the pH values measured by the pH meter and the fluorescent probes along with their standard deviations. In all cases, deviation of the measurements performed by the fluorescent probes were less then 5.00% with respect to the results of the pH meter.

## Cross-Sensitivity of the SDA and SDC towards Potential Interferents

The cross-sensitivity of the SDA and SDC towards $Na^+$, $K^+$, $Ca^{2+}$, $Mg^{2+}$ and $NH_4^+$and many other polyvalent metal ions was investigated in separate solutions for three replicate measurements. Among them interference effects of $Ca^{2+}$, $Mg^{2+}$, $Na^+$, $K^+$ and $NH_4^+$ is quite important because these ions are found to be almost all types of samples including biological fluids, drinking water, river and sea water [27, 28]. Both the SDA and SDC exhibited less than 5% relative signal change when exposed to the $10^{-3}$ M solutions of the conventional ions in water samples with negligible standard deviations. Similarly, emission based relative signal changes of $Zn^{2+}$, $Hg^+$, $Hg^{2+}$, $Sn^{2+}$, $Ba^{2+}$, $Ni^{2+}$, $Co^{2+}$, $Cu^{2+}$, $Pb^{2+}$, $Cr^{3+}$, $Mn^{2+}$, $Fe^{2+}$ and $Fe^{3+}$ were reported after exposure to $10^{-3}$ M solutions. Except that of $Mn^{2+}$ (14.3%), $Fe^{3+}$ (11.6%) and $Cr^{3+}$(14.7%), standard errors were less than 5.0% for the SDA. The SDC exhibited a fluctuation in response towards $Fe^{2+}$. Figure 13 reveals intensity based response of the dyes towards the metal cations in phosphate buffered solutions at pH 7.00. The most notable source of interference to the pH sensitivity of the SDA and SDC is the quenching of the excited states by the cations of $Zn^{2+}$, $Cu^{2+}$, $Ag^+$, $Hg^+$, $Mn^{2+}$, and $Fe^{3+}$ at neutral pHs for the SDA. The SDC exhibited less intense relative signal change when exposed to the all of the potential interferents with respect to the SDA in similar conditions.

The cross sensitivity tests were also performed for the conventional anions of $F^-$, $Cl^-$, $Br^-$, $NO_2^-$, $NO_3^-$, $PO_4^{3-}$, $SO_4^{2-}$ and $HCO_3^-$. Among them only the bicarbonate caused 85% quenching in the signal intensity which is an expected effect and can be attributed to the variation of the pH to 8.00–8.50. For the others the response was less than 4%.

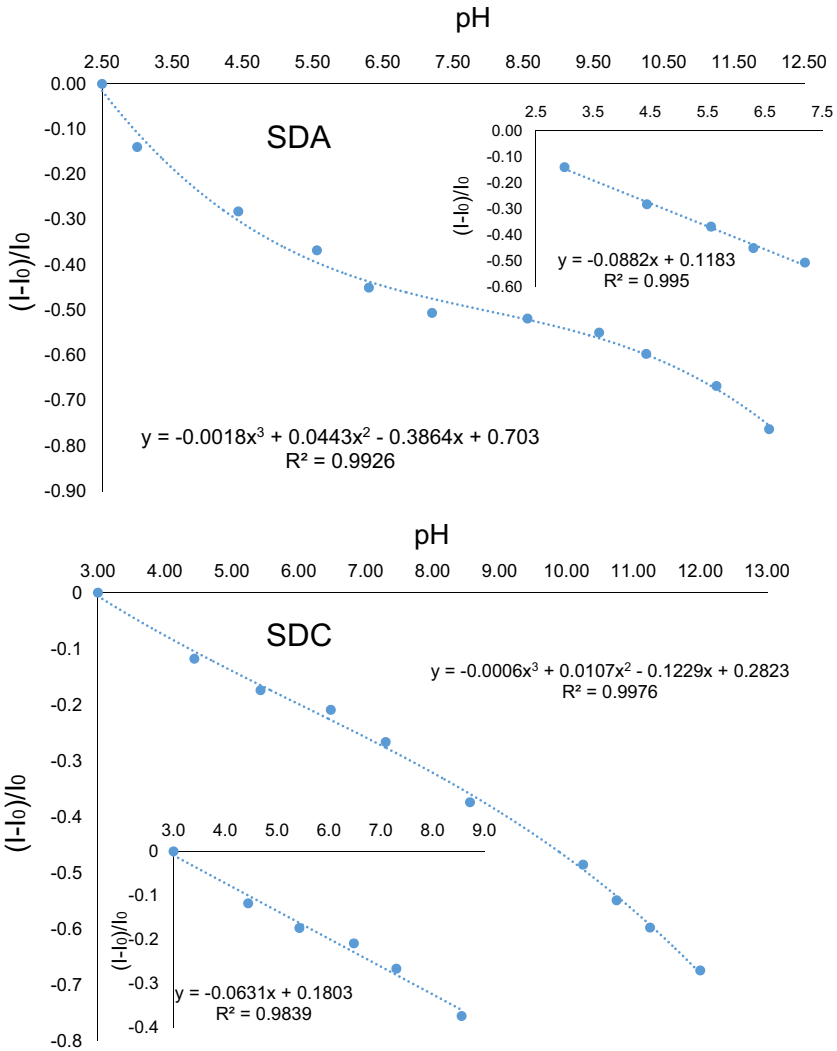


**Fig. 12** pH induced calibration plots of the SDA and SDC in Ag-doped electrospun fibers. Polynomial calibration plots were constructed using the spectral data given in Fig. 7-IV and Fig. 8 –II, respectively

## Conclusion

In this work, two different fluorescent dyes were embedded in polymeric matrices along with silver nanoparticles and an imidazolium based ionic liquid. The chosen dyes exhibited broad absorption bands covering most of the UV region, and, bright emission characteristics centered between 480 and 543 nm and 590–660 nm for the SDA and SDC, respectively. The long wavelength excitable dyes exhibited high quantum yields varying between 0.19–0.50 and large Stoke's shifts in the range of 45 and 80 nm. Herein, we investigated sensitivity of the two different fluorescent probes towards pH simulating harsh conditions with the saturated vapors of the strong acids of HCl, $HNO_3$ and $H_2SO_4$.

**Table 6** Comparative pH measurement results of the tap water samples by different approaches after addition of certain amounts of $10^{-3}$ M HCl solutions (for n = 3)

| Skiped Acid, μL ($10^{-3}$ M HCl) | pH of Tap water 25 C (Cond.:467 μS/cm, pH = 7.52) (pH meter) | pH of Tap water by SDA | Deviation from pH meter (%) | pH of Tap water by SDC | Deviation from pH meter (%) |
|---|---|---|---|---|---|
| 10 | 5.39 ± 0.19 | 5.27 ± 0.09 | −2.22 | 5.47 ± 0.14 | +3.79 |
| 50 | 4.69 ± 0.12 | 4.74 ± 0.11 | +1.06 | 4.56 ± 0.17 | −2.77 |
| 100 | 4.39 ± 0.21 | 4.29 ± 0.27 | −2.27 | 4.53 ± 0.11 | +3.19 |
| 150 | 4.22 ± 0.13 | 4.21 ± 0.16 | −0.23 | 4.16 ± 0.13 | −1.42 |
| 200 | 4.09 ± 0.08 | 4.01 ± 0.08 | +1.95 | 4.21 ± 0.12 | +2.93 |
| 300 | 3.92 ± 0.09 | 3.86 ± 0.08 | −1.52 | 3.88 ± 0.15 | −1.02 |

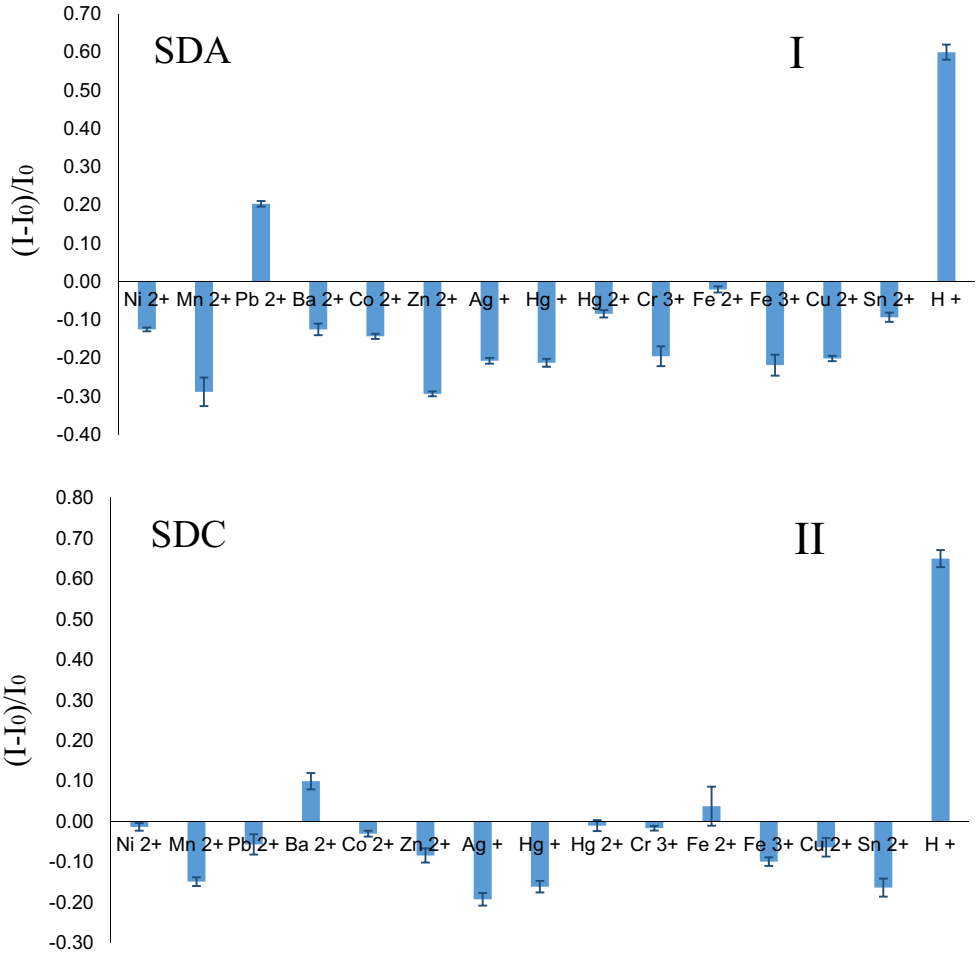


**Fig. 13** Metal-ion response test results for the EC embedded SDA and SDC. Results are plotted as relative fluorescence changes, (I-Io)/Io, where I is the fluorescence intensity of the sensor membrane after exposure to ion-containing solutions and Io is the fluorescence intensity of the sensor slide in ion-free buffer solution

Generally, the pH sensitive dyes become irreversibly poisoned when exposed to the vapors of strong acids and lose their sensitivity towards pH. Here we provided an extraordinary immunity on the pH sensitivity of the fluorescent pH probes utilizing AgNPs and ionic liquid together within the same matrix. We obtained high sensitivity when used these additives in appropriate amounts. We provided enhanced stability and securely entrapped the dye molecules without any leaching from the polymeric matrices. The offered composites can be employed for pH measurements even in environments occupied by concentrated acid vapors of well-known strong mineral and oxidizing acids. We also tested the fabricated materials with naked eye in plastic syringes for practical applications, successfully.

**Acknowledgements** We gratefully acknowledge that funding of this project was provided by the Scientific and Technological Research Council of Turkey (TUBITAK) (Research Fellowship Program for National Researchers, 2210-C). We also thank to the Scientific Research Funds of Dokuz Eylul University (project number: 2014. KB. FEN.040).

## References

1. Tian Y, Fuller E, Klug S, Lee F, Su F, Zhang L, Chao S, Meldrum D (2013) A fluorescent colorimetric pH sensor and the influences of matrices on sensing performances. Sens Actuators B Chem 188:1–10
2. Veselov A, Thur C, Efimov A, Guina M, Lemmetyinen H, Tkachenko N (2010) Acidity sensor based on porphyrin self-assembled monolayers covalently attached to the surfaces of tapered fibres. Meas Sci Technol 21:115–205
3. Schulman GS, Chen S, Bai F, Leiner MJP, Weis L, Wolfbeis OS (1995) Dependence of the fluorescence of immobilized 1-hydroxypyrene-3,6-trisulfonate on solution pH: extension of the range of applicability of a pH fluorosensor. Anal Chim Acta 304: 165–170
4. Wencel D, Barczak M, Borowski P, McDonagh C (2012) The development and characterization of novel hybrid sol–gel-derived films for optical pH sensing. J Mater Chem 22:117–120
5. Bai Z, Chen R, Si P, Huang Y, Sun H, Kim DH (2013) Fluorescent pH sensor based on Ag@$SiO_2$ core–shell nanoparticle. ACS Appl Mater Interfaces 5:5856–5860
6. Cui Q, Podrazký O, Mrázek J, Proboštová J, Kašík I (2015) Tapered-fiber optical sensor for physiological pH range. IEEE Sensors J 15:4967–4973

7. Ray A, Lee YEK, Epstein T, Kim G, Kopelman R (2011) Two-photon nano-PEBBLE sensors: subcellular pH measurements. Analyst 136:3616–3622
8. Kermis RH, Kostov Y, Rao G (2003) Rapid method for the preparation of a robust optical pH sensor. Analyst 128:1181–1186
9. Lobnik A, Oehme I, Murkovic I, Wolfbeis OS (1998) pH optical sensors based on sol-gels: chemical doping versus covalent immobilization. Anal Chim Acta 367:159–165
10. Dorota W, Abel T, McDonagh C (2014) Optical chemical pH sensors. Anal Chem 86:15–29
11. Marcosa S, Wolfbeis OS (1996) Optical sensing of pH based on polypyrrole films. Anal Chim Acta 334:149–153
12. Koncki R, Wolfbeis OS (1999) Composite films of Prussian blue and n-substituted polypyrroles: covalent immobilization of enzymes and application to near infrared optical biosensing. Biosens Bioelectron 14:87–92
13. Liebsch G, Klimant I, Krause C, Wolfbeis OS (2001) Fluorescent imaging of pH with optical sensors using time domain dual lifetime referencing. Anal Chem 73:4354–4363
14. Weidgans BM, Krause C, Klimant I, Wolfbeis OS (2004) Fluorescent pH sensors with negligible sensitivity to ionic strength. Analyst 129:645–650
15. Aigner D, Borisov SM, Klimant I (2011) New fluorescent perylene bisimide indicators a platform for broadband pH optodes. Anal Bioanal Chem 400:2475–2485
16. Aigner D, Borisov SM, FJO F, JFF S, Saf R, Klimant I (2012) New fluorescent pH sensors based on covalently linkable PET rhodamines. Talanta 99:194–201
17. Shiraishi T, Saito T, Kagechika H, Hirano T (2014) Development of a novel fluorescent sensor to detect a specific range of pH. Tetrahedron Lett 55:6784–6786
18. Zhao Y, Zhang G, Liu Z, Li P (2016) Benzimidazo[2,1-a]benz[de]isoquinoline-7-one-12-carboxylic acid based fluorescent sensors for pH and $Fe^{3}$+. J Photochem Photobiol 314:52–59
19. Kacmaz S, Ertekin K, Oter O, Hızlıateş CG, Ergun Y, Celik E (2015) Manipulation of induced sensitivity of a fluorescent probe in presence of silver nanoparticles. J Lumin 168:228–235
20. Derinkuyu S, Ertekin K, Oter O, Denizalti S, Cetinkaya E (2008) Emission based fiber optic pH sensing with Schiff bases bearing dimethylamino groups. Dyes Pigments 76:133–141
21. Nesterov VN, Timofeeva TV, Borbulevych OY, Antipin MY, Clark RD (2000) 2-Amino derivatives of 5-nitrophenylacetamide. Acta Crystallographica Section C Crystal Struct Commun 56:971–977
22. Solomon SD, Bahadory M, Jeyarajasingam AV, Rutkowsky SA, Boritz C (2007) Synthesis and study of silver nanoparticles. J Chem Educ 8:322–326
23. Derinkuyu S, Ertekin K, Oter O, Denizalti S, Cetinkaya E (2007) Fiber optic pH sensing with long wavelength excitable Schiff bases in the pH range of 7.0-12.0. Anal Chim Acta 588:42–49
24. Wolfbeis OS (1990) Fiber optic chemical sensors and biosensors. CRC Press, Boca Raton, Fla (1-2)
25. Oter O, Ertekin K, Derinkuyu S (2009) Photophysical and optical oxygen sensing properties of tris(bipyridine)ruthenium(II) in ionic liquid modified sol-gel matrix. Mater Chem Phys 113:322–328
26. Aydogdu S, Ertekin K, Suslu A, Ozdemir M, Celik E, Cocen U (2011) Optical $CO_2$ sensing with ionic liquid doped electrospun nanofibers. J Fluoresc 21:607–613
27. Wang E, Zhou Y, Huang Q, Pang L, Qiao H, Yu F (2016) 5-Hydroxymethylfurfural modified rhodamine B dual-function derivative: highly sensitive and selective optical detection of pH and $Cu^{2+}$. Spectrochim Acta A Mol Biomol Spectrosc 152:327–335
28. Feng Y, Liu Y, Su C, Ji X, He Z (2014) New fluorescent pH sensor based on label free silicon nanodots. Sens Actuators B Chem 203: 795–801